FRONTIERS OF PHYSICS

RESEARCH ARTICLE
Volume 17 / Issue 6 / 63508 / 2022

Equipartition of current in metallic armchair nanoribbon of graphene-based device

Hui Yang[1], Junjie Zeng[1], Sanyi You[1], Yulei Han[2,†], Zhenhua Qiao[1,3,‡]

1 CAS Key Laboratory of Strongly-Coupled Quantum Matter Physics, and Department of Physics, University of Science and Technology of China, Hefei 230026, China
2 Department of Physics, Fuzhou University, Fuzhou 350108, China
3 ICQD, Hefei National Research Center for Physical Sciences at the Microscale, University of Science and Technology of China, Hefei 230026, China
Corresponding authors. E-mail: †hanyulei@ustc.edu.cn, ‡qiao@ustc.edu.cn
Received April 27, 2022; accepted August 11, 2022

ABSTRACT

We numerically investigate the mesoscopic electronic transport properties of Bernal-stacked bilayer/trilayer graphene connected with four monolayer graphene terminals. In armchair-terminated metallic bilayer graphene, we show that the current from one incoming terminal can be equally partitioned into other three outgoing terminals near the charge-neutrality point, and the conductance periodically fluctuates, which is independent of the ribbon width but influenced by the interlayer hopping energy. This finding can be clearly understood by using the wave function matching method, in which a quantitative relationship between the periodicity, Fermi energy, and interlayer hopping energy can be reached. Interestingly, for the trilayer case, when the Fermi energy is located around the charge-neutrality point, the fractional quantized conductance $1/(4e^2/h)$ can be achieved when system exceeds a critical length.

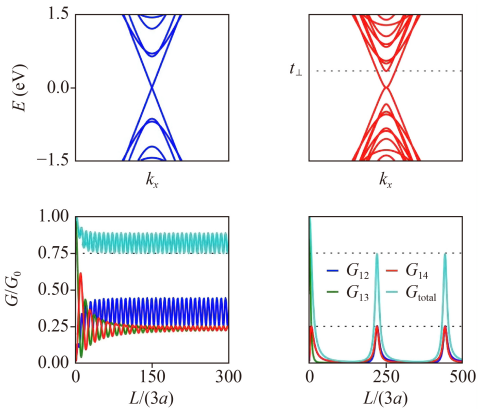

Keywords graphene, electronic transport, armchair nanoribbon

1 Introduction

The research of two-dimensional layered materials has attracted great attention [1–18]. Graphene, in particular, has been made into a variety of electronic devices and is a promising candidate in spintronics because of its excellent thermal and electronic properties [19–34]. Compared with monolayer graphene, multilayer graphene shows more complex phenomena due to the modification of energy dispersion by interlayer interaction. Previous studies on the electronic transport properties in multilayer graphene mainly focused on the planar properties, such as quantum anomalous Hall effect, nonlocal electron transport in bilayer graphene, and intervalley scattering in magic-angle graphene [35–38].

The layer of graphene can provide another adjustable freedom degree and interlayer interaction can change the distribution of charges between different layers. Due to the torsion of angle and interlayer distance between different layers, there will be significant differences in the electrical resistance [23, 39]. Investigations have been made to explore the transmission through the boundary between (two) monolayer and bilayer graphene from tight binding model or by analytical method [40–50]. High tunability of transport properties in such a configuration was revealed, while around the Dirac point, the Fano factor has the 1/3 value characteristic of diffusive transport [44]. Experimentally, it is easier for the Bernal-stacked multilayer graphene to be mechanically peeled from graphite, where only half atoms in one layer

Higher Education Press

https://doi.org/10.1007/s11467-022-1201-2

exit hopping with adjacent layers [51–54]. The armchair nanoribbons are cut from graphene and basically maintain the two-dimensional plane structure of graphene. However, for zigzag nanoibbon, its edge states exert a great influence on tranposrt properties and are sensitive to edges roughness [55, 56].

In this work, we systematically study the electronic transport properties of bilayer or trilayer graphene with armchair edges contacted with four monolayer graphene terminals. When current is injected into bilayer region from one monolayer terminal, the incident current is equally distributed in the remaining terminals when the Fermi energy is close to the charge neutrality point ($E_F < 0.001$ eV). An obvious periodicity of conductance variation between insulating and conducting states can be observed as a function of central scattering region length. The resonance of wave functions leads to a conductance peak of $0.25e^2/h$, indicating that the incident current is split evenly by the multilayer device. The above phenomena are independent of metallic nanoribbon width but are influenced by interlayer hopping energy. In the case of trilayer graphene, when the Fermi energy is close enough to the charge-neutrality point ($E_F < 0.001$ eV), there is a quasi-platform ($0.25e^2/h$) with the central region length increasing. At the resonance peak, only one of the outgoing terminals is conductive and others are insulating. The total transmission keeps $0.75e^2/h$ between the two peaks of conductance and approaches e^2/h at the peak of the conductance. Our work provides an effective method of controlling the electron transmittance only by adjusting the sample size and Fermi energy.

2 System models and methods

To study the resonance in multilayer graphene, we construct the device as shown in Fig. 1(a), where the red represents the central scattering region and the blue denotes four semi-infinite monolayer graphene leads

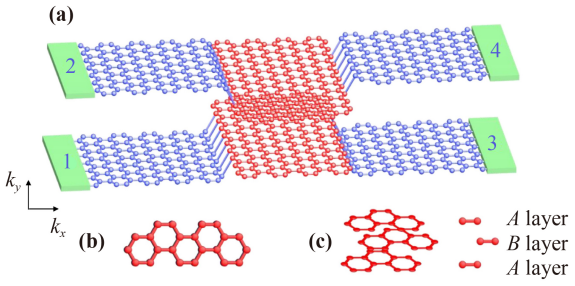

Fig. 1 **(a)** Schematic diagram of the bilayer graphene device. The red part is central scattering region where exits interlayer hopping $t_\perp = 0.34$ eV. The four blue regions are infinite monolayer graphene reservoirs and current is incident from terminal 1. **(b)** Graphene nanoribbon with armchair boundary. **(c)** Side view of ABA-stacked trilayer graphene.

labeled as i ($i = 1, 2, 3, 4$), with current injected from terminal 1. The central scattering regions are AB-stacked bilayer and ABA-stacked trilayer with armchair edges, respectively [see Figs. 1(b) and (c)]. The width and length of nanoribbon are measured by the number of atoms in the transverse direction and the number of unit cells in the machine direction, respectively. The π-band tight-binding Hamiltonian of the system can be written as

$$H = \sum_{\langle i,j \rangle} \gamma_{i,j}\, c_i^\dagger c_j, \tag{1}$$

where $c_i^\dagger$ (c_j) is the creation (annihilation) operator at site i. The hopping amplitude $\gamma_{i,j}$ is defined as $t = -2.6$ eV ($t_\perp = 0.34$ eV) for the nearest-neighbor sites in the same layer (different layers). The electronic transport properties are investigated by calculating the conductance between terminals q and p, which can be described by the Landauer–Büttiker formula [57]:

$$G_{pq} = \frac{e^2}{h} \mathrm{Tr}\left[\Gamma_q G^{\mathrm{r}} \Gamma_p G^{\mathrm{a}}\right], \tag{2}$$

where $G^{\mathrm{r}\,(\mathrm{a})}$ is the retarded (advanced) Green's function of the central scattering region, and $\Gamma_{q/p}$ is the line-width function coupling the terminal to the central region.

3 Results in AB-stacked bilayer graphene

We first investigate the electronic transport properties in AB-stacked bilayer graphene. The electronic property of an armchair nanoribbon is determined by its width, i.e., semi-metallic for nanoribbon width of $3m + 2$ (m is a positive integer) and insulating for other widths. Therefore, in our calculations, the ribbon width is set to be 20 to keep a metallic state. The corresponding one-dimensional band structures are plotted in Fig. 2(a). One can find that the monolayer graphene lead displays linear energy dispersion whereas the bilayer graphene central region demonstrates quadratic dispersion in low-energy range of $|E| \le t_\perp$ due to interlayer interaction [see Figs. 2(a) and (b)].

We then study the four-terminal conductance variation as a function of length of the bilayer central region at a certain Fermi energy. When $|E_F| > t_\perp$, interference between conduct channels leads to antiresonance phenomenon (see Appendix for more information), i.e., the G_{13} approaches its maximum while the G_{14} reaches its minimum. The conductance from terminal 1 to other terminals have an obvious period, which is similar to the results reported in the step monolayer-bilayer graphene junctions [48],where the electronic transmission through the central region depends on the position of the mono-layerlayer port connected in the central region.

When $|E_F| < t_\perp$, one can find one conducting channel

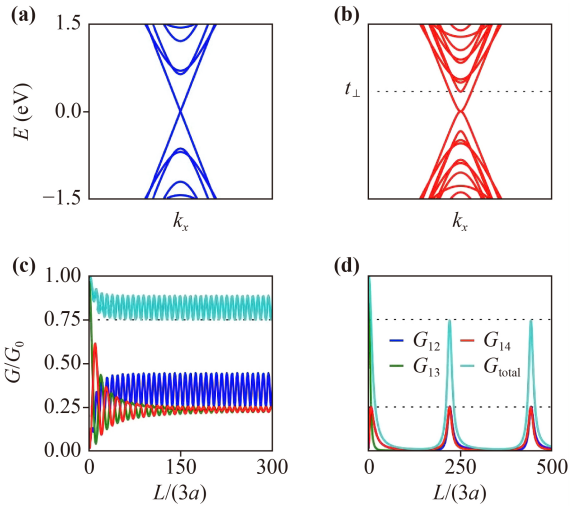

Fig. 2 Energy bands for graphene nanoribbon with open boundary only in y direction. The blue dispersion corresponds to monolayer graphene and the red part describes bilayer graphene bands. **(a, b)** Nanoribbon with width set to be 20 atoms terminates in armchair boundary. **(c, d)** Conductance as a function of central scattering length L for armchair terminated bilayer graphene with $E_{\text{F}} = 0.339$ eV and $E_{\text{F}} = 0.001$ eV. Dashed lines in (d) represent $0.25G_0$ and $0.75G_0$.

from Fig. 2(b) in the central bilayer region, and the conductance antiresonance between G_{13} and G_{14} gradually disappears as the length of the bilayer central region increases. For example, Fig. 2(c) displays the four-terminal conductance as a function of central scattering length L for armchair terminated bilayer graphene with $E_{\text{F}} = 0.339$ eV. We can see that, while G_{13} and G_{14} have antiresonance behavior for shorter L, they are nearly equal for longer L, with a peak of roughly 0.25 e^2/h. The conductance G_{12} also has a clear period, and the valley value is 0.25 e^2/h, which is identical to the peak values of G_{13} and G_{14}.

When E_{F} is shifted from the second sub-band edge to the charge-neutrality point, as shown in Fig. 2(d), G_{1i} $(i = 2, 3, 4)$ exhibits pulse-wave-like period with a periodic length of $L \approx 663a$ where $a = 1.42$ Å is the lattice constant of graphene. The conductance peak of G_{1i} $(i = 2, 3, 4)$ is around 0.25 e^2/h, and the incident current is split equally by this device. Considering $G_{11} + G_{12} + G_{13} + G_{14} = e^2/h$ and $G_{\text{total}} = 0.75\, e^2/h$ at the peak, we can deduce that a quarter of current bounces back to the incident terminal. Moreover, between the two adjacent peaks, G_{1i} $(i = 2, 3, 4) \approx 0$ indicates that the entire system is almost an insulator, with the majority of current reflected back to the incident terminal. We also find that the length period of conductance variation is independent of nanoribbon width, but can be tuned by adjusting the Fermi energy or interlayer hopping energy, i.e., the closer the Fermi energy to charge neutrality point or the less interlayer hopping energy, the longer the period. We employ the low-energy effective Hamiltonian to explain the above phenomena. The effective Hamiltonian of monolayer graphene near the Dirac cone can be described as

$$H = \begin{pmatrix} 0 & q_x + \mathrm{i}q_y \\ q_x - \mathrm{i}q_y & 0 \end{pmatrix}, \tag{3}$$

where q_x (q_y) is the momentum in x (y) direction. The eigenvector corresponding to the eigenvalue E of H is

$$f = \frac{1}{\sqrt{2}E} \begin{pmatrix} E \\ q_x + \mathrm{i}q_y \end{pmatrix} \tag{4}$$

for the incident particle, the relation between energy and momentum satisfies $E^2 = q_x^2 + q_y^2$.

The low-energy effective Hamiltonian of Bernal-stacked bilayer graphene in one valley is written as

$$H_{\text{BLG}} = \begin{pmatrix} 0 & k_x + \mathrm{i}k_y & t_\perp & 0 \\ k_x - \mathrm{i}k_y & 0 & 0 & 0 \\ t_\perp & 0 & 0 & k_x - \mathrm{i}k_y \\ 0 & 0 & k_x + \mathrm{i}k_y & 0 \end{pmatrix}, \tag{5}$$

where (k_x, k_y) is the momentum, and the corresponding spinor of Hamiltonian is $\phi = (\phi_{A_1}, \phi_{B_1}, \phi_{A_2}, \phi_{B_2})^{\text{T}}$. The eigenvector corresponding to the eigenvalue E of H_{BLG} is

$$f_{\text{B}} = \begin{pmatrix} (E^2 - k_x^2 - k_y^2)E \\ (E^2 - k_x^2 - k_y^2)(k_x - \mathrm{i}k_y) \\ t_\perp E^2 \\ t_\perp E(k_x + \mathrm{i}k_y) \end{pmatrix}, \tag{6}$$

where E satisfies

$$k_x^2 = E^2 \pm t_\perp E - k_y^2. \tag{7}$$

As mentioned in previous studies [40, 47], for metallic armchair nanoribbon, we can incident the particle in the lowest energy sub-band from monolayer graphene to bilayer graphene, and view the central region as a potential well. Then the conductance can be calculated by matching wave function in the boundary. The incident wave function in terminal 1 can be set as

$$\psi_1 = f\mathrm{e}^{\mathrm{i}q_x x} + rf\mathrm{e}^{-\mathrm{i}q_x x}, \tag{8}$$

where r is reflection amplitude. In other terminals, the wave functions are written as

$$\psi_2 = t_2 f\mathrm{e}^{-\mathrm{i}q_x x}, \tag{9}$$

$$\psi_3 = t_3 f\mathrm{e}^{\mathrm{i}q_x x}, \tag{10}$$

$$\psi_4 = t_4 f\mathrm{e}^{\mathrm{i}q_x x}, \tag{11}$$

where t_i $(i = 2, 3, 4)$ are the transmission amplitudes to the corresponding terminals. In the bilayer graphene, there are four solutions of Eq. (7) for k_x, which can be identified as $\pm k_{x1}$ and $\pm k_{x2}$. Inside the bilayer region, the wave function is the linear combination of the eigenfunc-

tions with different momentums, which can denoted as

$$\psi = a_1 f_B e^{ik_{x1}x} + a_2 f_B e^{ik_{x2}x} + a_3 f_B e^{-ik_{x1}x} + a_4 f_B e^{-ik_{x2}x}. \quad (12)$$

For the normal incident current at the low-energy region ($E \to 0$), there are two traveling modes with momentums of $\pm\sqrt{t_\perp E}$, and two evanescent modes with momentums of $\pm\sqrt{t_\perp E}$i. Combining wave functions with the boundary conditions, i.e., wave functions are continuous in the boundary between monolayer and bilayer graphene, we can obtain the transmission coefficient, which is the same as the results from tight-binding model. The four wave functions intervene in the bilayer graphene region, resulting in a periodic oscillation phenomena. The oscillation period is $\pi/k_{x1} = \pi/\sqrt{t_\perp E}$, indicating that we can control the period by changing interlayer interaction or Fermi energy.

To clearly understand the behavior of electron, we plot the wave function distribution as a function of bilayer graphene length x in the central region. As displayed in Fig. 3(a), with fixed central scattering region length $L = 546a$, in the left boundary between terminal 1 and bilayer graphene, the wave function is mainly distributed in the atom B_1, so for the incident electron which equally distributes in the A_1, B_1, it would reflect back to incident terminal completely. For length $L = 663a$ where conductance comes to a peak, in the left boundary between terminal 1 and bilayer graphene, the electron would also distribute in the other atoms and three-fourths currents transmit over the barrier. In other three boundaries, the wave function distributes equally in two atoms A_i, B_i $(i = 1, 2)$, so the transmitted current will be evenly distributed in three outgoing terminals.

4 Results in trilayer graphene

Here, we turn to explore the conductance variation in ABA-stacked trilayer graphene near the charge-neutrality point. First we plot the armchair nanoribbon band structure of trilayer graphene in Fig. 4(a). One can find two sub-bands in low energy region, i.e., one is linear and the other is quadratic, leading to different transport phenomena. The interference between these two sub-bands results in antiresonance behavior which is the same as that in bilayer graphene. Figures 4(b)–(d) display the conductance as a function of central scattering length L for armchair terminated trilayer graphene with different Fermi energies. For $E_F = 0.001$ eV as shown in Fig. 4(b), with the increasing of L, all the conductance first quickly approaches a quasi plateau of $0.25\, e^2/h$, then the conductance G_{12} and G_{13} rapidly diminish to zero at the first resonance length, while G_{14} reaches its maximum of e^2/h. As L further increases, all the conductance keeps around $0.25\, e^2/h$ before reaching the second resonance length. At the second resonance point, G_{12} and G_{14} nearly vanishes whereas G_{13} reaches e^2/h. Then the conductance oscillates repeatedly with L. At larger L, the conductance G_{13} and G_{14} gradually deviate from the plateau of $0.25\, e^2/h$, whereas the conductance G_{12} always keeps $0.25\, e^2/h$. It is worth noting that the total transmission is 0.75, indicating the reflection probability is 0.25, which is the same as that in bilayer graphene. We can control the oscillation period between two resonance peaks by tuning the Fermi energy, i.e., the first conductance plateau will increase more than $2100a$ when the Fermi energy is located at $E_F = 0.0001$ eV and $E_F = 0.00001$ eV, providing a strategy to split current evenly [see Figs. 4(c) and (d)]. For undoped trilayer graphene, this device theoretically split equally injected current.

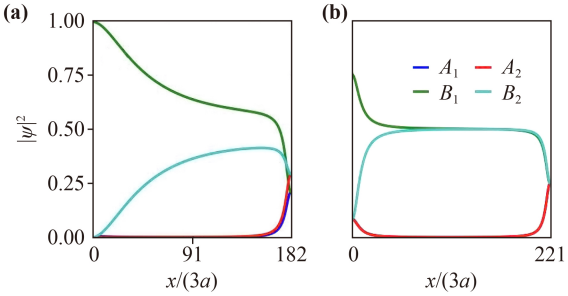

Fig. 3 Probability distribution of wave function as a function of bilayer graphene length x with fixed Fermi energy $E_F = 0.001$ eV. **(a, b)** The central region length are set to be $546a$ and $663a$ respectively.

5 Summary and discussion

We systematically investigate the electronic transport properties in armchair-terminated bilayer and trilayer graphene from tight-binding model and wave function matching method. In low energy, different dispersion

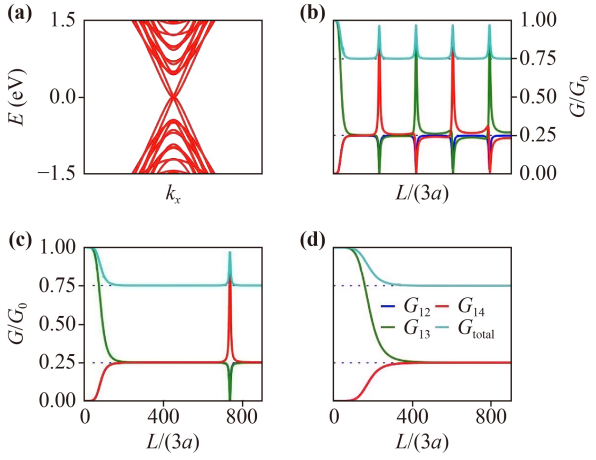

Fig. 4 **(a)** Ribbon band structure of ABA-stacked trilayer graphene. Conductance as a function of central scattering length L for armchair terminated trilayer graphene with **(b)** $E_F = 0.001$ eV, **(c)** $E_F = 0.0001$ eV, **(d)** $E_F = 0.00001$ eV. The nanoribbon width is set to be 20 atoms. The dashed blue lines represent $0.25G_0$ and $0.75G_0$.

results in various current distribution phenomena. Wave functions with different momenta in central scattering region intervene with each other, which leads to a periodic change in conductance. In armchair-terminated bilayer graphene nanoribbon, incident current flows equally to the outgoing terminals, and at the peak, the conductance is $0.25\,e^2/h$. In armchair-terminated trilayer graphene, as long as the Fermi energy is close to the charge-neutrality point, a quasi-platform ($0.25\,e^2/h$) appears with the increasing of length. With the help of this four-terminal device, we could control electron transmission by Fermi energy and sample size. What is even more interesting is that we could realize the even split of current. Here, there is no applied external voltage in those systems and the only condition is that Fermi energy is near charge-neutrality point, which could be realized easily in experiment. Near the low energy level, as long as the energy band structure is similar to that of bilayer graphene, the periodic regulation of current can be realized through a similar bilayer structure with the help of interlayer coupling strength.

Acknowledgements This work was financially supported by the National Natural Science Foundation of China (Grant Nos. 11974327 and 12004369), the Fundamental Research Funds for the Central Universities (Nos. WK3510000010 and WK2030020032), Anhui Initiative in Quantum Information Technologies (Grant No. AHY170000). We also thank the supercomputing service of AM-HPC and the Supercomputing Center of University of Science and Technology of China for providing the high performance computing resources.

Appendix A

When the Fermi energy $E_F > t_\perp$, the conductance variation as a function of central region length is depicted in Fig. A1. The total conductance is related to the number of channels. Due to scattering between multiple channels, G_{13} and G_{14} are complementary, and the value of G_{12} is not zero, indicating that a certain current flows into terminal 2.

We also calculated the variation of the conductance when the central scattering region is zigzag boundary graphene. Figure A2 shows the zigzag ribbon band

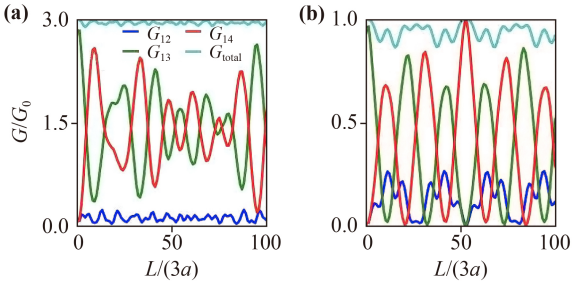

Fig. A1 **(a, b)** Conductance as a function of central scattering length L for armchair terminated bilayer graphene with $E_F = 1$ eV and $E_F = 0.4$ eV.

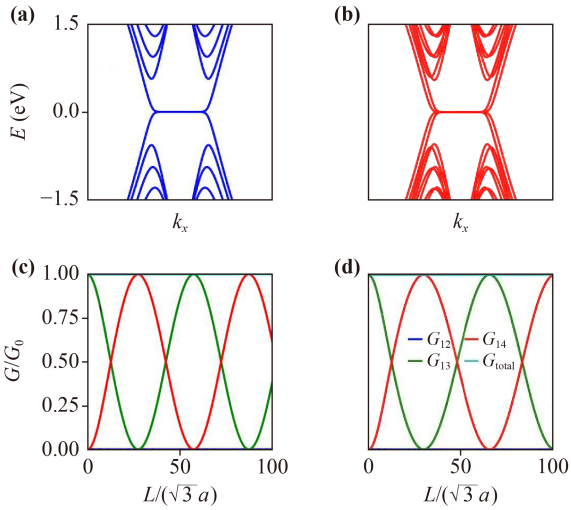

Fig. A2 Energy bands for graphene nanoribbon with open boundary only in y direction. The blue dispersion corresponds to monolayer graphene and the red part describes bilayer graphene bands. **(a, b)** Nanoribbon with width set to be 20 atoms terminates in zigzag boundary. **(c, d)** Conductance as a function of central scattering length L for zigzag terminated bilayer graphene with width 20 and 40 atoms.

structure of monolayer graphene and AB-stacked bilayer graphene. In the low energy, there are two conductive channels in bilayer graphene. When the central scattering region is AB-stacked zigzag bilayer graphene, due to the intervention between these two channels, the conductance $G_{1i}(i = 2, 3, 4)$ changes periodically. The sum of G_{13} and G_{14} has always been e^2/h. When G_{14} reaches the maximum, G_{13} becomes the minimum and vice versa. The changing period of conductance is related to the ribbon width. The wider the strip is, the longer the change period will be.

Appendix B

The result calculated by the continuous model is shown in Fig. B1. The Fermi energy is set to be 0.001 eV. We can find that $T_{1i}(i = 2, 3, 4)$ shows obvious periodic

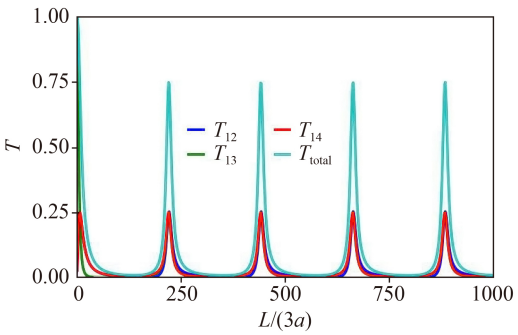

Fig. B1 This is the result obtained from the continuous model. The Fermi energy is 0.001 eV. The maximum value of transmission probability T_{1i} (i=2, 3, 4) is still around 0.25.

change, and the whole system changes into conductor and insulator state as the length of the central region changes. The period of transmission probability is $\pi/k_{x1} = \pi/\sqrt{t_\perp E}$, which indicates that it is only related to the interlayer coupling strength and the incident electron energy. The values of transmission probability are almost the same, indicating that the device has achieved the equal distribution of current. This result is consistent with the result calculated by Landauer–Büttiker formula.

References

1. M. Xu, T. Liang, M. Shi, and H. Chen, Graphene-like two-dimensional materials, *Chem. Rev.* 113(5), 3766 (2013)
2. Q. H. Wang, K. Kalantar-Zadeh, A. Kis, J. N. Coleman, and M. S. Strano, Electronics and optoelectronics of two-dimensional transition metal dichalcogenides, *Nat. Nanotechnol.* 7(11), 699 (2012)
3. K. S. Novoselov, D. Jiang, F. Schedin, T. J. Booth, V. V. Khotkevich, S. V. Morozov, and A. K. Geim, Two-dimensional atomic crystals, *Proc. Natl. Acad. Sci. USA* 102(30), 10451 (2005)
4. Y. L. Han and Z. H. Qiao, Universal conductance fluctuations in Sierpinski carpets, *Front. Phys.* 14(6), 63603 (2019)
5. S. Zhou, L. You, H. Zhou, Y. Pu, Z. Gui, and J. Wang, Van der Waals layered ferroelectric $CuInP_2S_6$: Physical properties and device applications, *Front. Phys.* 16(1), 13301 (2021)
6. H. Z. Lu and S. Q. Shen, Quantum transport in topological semimetals under magnetic fields, *Front. Phys.* 12(3), 127201 (2017)
7. H. Dong, S. Guo, Y. Duan, F. Huang, W. Xu, and J. Zhang, Electronic and optical properties of single-layer MoS_2, *Front. Phys.* 13(4), 137307 (2018)
8. X. R. Hu, J. M. Zheng, and Z. Y. Ren, Strong interlayer coupling in phosphorene/graphene van der Waals heterostructure: A first-principles investigation, *Front. Phys.* 13(2), 137302 (2018)
9. Y. Ren, Z. Qiao, and Q. Niu, Topological phases in two-dimensional materials: A review, *Rep. Prog. Phys.* 79(6), 066501 (2016)
10. X. T. Bi, J. Jung, and Z. H. Qiao, Role of geometry and topological defects in the one-dimensional zero-line modes of graphene, *Phys. Rev. B* 92(23), 235421 (2015)
11. K. Wang, Y. F. Ren, X. Z. Deng, S. A. Yang, J. Jung, and Z. H. Qiao, Gate-tunable current partition in graphene-based topological zero lines, *Phys. Rev. B* 95(24), 245420 (2017)
12. Z. H. Qiao, J. Jung, C. Lin, Y. F. Ren, A. H. MacDonald, and Q. Niu, Current partition at topological channel intersections, *Phys. Rev. Lett.* 112(20), 206601 (2014)
13. Z. H. Qiao, J. Jung, Q. Niu, and A. H. MacDonald, Electronic highways in bilayer graphene, *Nano Lett.* 11(8), 3453 (2011)
14. T. Hou, G. Chen, W. K. Tse, C. Zeng, and Z. Qiao, Topological zero-line modes in folded bilayer graphene, *Phys. Rev. B* 98(24), 245417 (2018)
15. X. Y. Peng and R. Ahuja, Symmetry breaking induced bandgap in epitaxial graphene layers on SiC, *Nano Lett.* 8(12), 4464 (2008)
16. G. Giovannetti, P. A. Khomyakov, G. Brocks, P. J. Kelly, and J. van den Brink, Substrate-induced band gap in graphene on hexagonal boron nitride: *Ab initio* density functional calculations, *Phys. Rev. B* 76(7), 073103 (2007)
17. W. Yao, S. A. Yang, and Q. Niu, Edge states in graphene: From gapped flat-band to gapless chiral modes, *Phys. Rev. Lett.* 102(9), 096801 (2009)
18. K. S. Novoselov, A. K. Geim, S. V. Morozov, D. Jiang, Y. Zhang, S. V. Dubonos, I. V. Grigorieva, and A. A. Firsov, Electric field effect in atomically thin carbon films, *Science* 306(5696), 666 (2004)
19. Y. Zhang, Y. W. Tan, H. L. Stormer, and P. Kim, Experimental observation of the quantum Hall effect and Berry's phase in graphene, *Nature* 438(7065), 201 (2005)
20. C. W. J. Beenakker, Andreev reflection and Klein tunneling in graphene, *Rev. Mod. Phys.* 80(4), 1337 (2008)
21. A. H. Castro Neto, F. Guinea, N. M. R. Peres, K. S. Novoselov, and A. K. Geim, The electronic properties of graphene, *Rev. Mod. Phys.* 81(1), 109 (2009)
22. S. Y. Zhou, G. H. Gweon, A. V. Fedorov, P. N. First, W. A. de Heer, D. H. Lee, F. Guinea, A. H. Castro Neto, and A. Lanzara, Substrate-induced bandgap opening in epitaxial graphene, *Nat. Mater.* 6(10), 770 (2007)
23. K. M. M. Habib, S. S. Sylvia, S. Ge, M. Neupane, and R. K. Lake, The coherent interlayer resistance of a single, rotated interface between two stacks of AB graphite, *Appl. Phys. Lett.* 103(24), 243114 (2013)
24. S. Ge, K. M. M. Habib, A. De, Y. Barlas, D. Wickramaratne, M. R. Neupane, and R. K. Lake, Interlayer transport through a graphene/rotated boron nitride/graphene heterostructure, *Phys. Rev. B* 95(4), 045303 (2017)
25. F. Xia, D. B. Farmer, Y. Lin, and P. Avouris, Graphene field-effect transistors with high On/Off current ratio and large transport band gap at room temperature, *Nano Lett.* 10(2), 715 (2010)
26. Y. Kim, H. Yun, S. G. Nam, M. Son, D. S. Lee, D. C. Kim, S. Seo, H. C. Choi, H. J. Lee, S. W. Lee, and J. S. Kim, Breakdown of the interlayer coherence in twisted bilayer graphene, *Phys. Rev. Lett.* 110(9), 096602 (2013)
27. E. McCann and M. Koshino, The electronic properties of bilayer graphene, *Rep. Prog. Phys.* 76(5), 056503 (2013)
28. K. Wang, T. Hou, Y. F. Ren, and Z. H. Qiao, Enhanced robustness of zero-line modes in graphene via magnetic field, *Front. Phys.* 14(2), 23501 (2019)
29. R. Wang, X. Ren, Z. Yan, L. J. Jiang, W. E. I. Sha, and G. C. Shan, Graphene based functional devices: A short review, *Front. Phys.* 14(1), 13603 (2019)
30. X. Z. Deng, H. L. Yang, S. F. Qi, X. H. Xu, and Z. H. Qiao, Quantum anomalous Hall effect and giant Rashba spin–orbit splitting in graphene system co-doped with boron and 5d transition-metal atoms, *Front. Phys.* 13(5), 137308 (2018)

31. L. J. Yin, K. K. Bai, W. X. Wang, S. Y. Li, Y. Zhang, and L. He, Landau quantization of Dirac fermions in graphene and its multilayers, *Front. Phys.* 12(4), 127208 (2017)
32. J. L. Ge, T. R. Wu, M. Gao, Z. B. Bai, L. Cao, X. F. Wang, Y. Y. Qin, and F. Q. Song, Weak localization of bismuth cluster-decorated graphene and its spin–orbit interaction, *Front. Phys.* 12(4), 127210 (2017)
33. W. Yan, S. Y. Li, L. J. Yin, J. B. Qiao, J. C. Nie, and L. He, Spatially resolving unconventional interface Landau quantization in a graphene monolayer-bilayer planar junction, *Phys. Rev. B* 93(19), 195408 (2016)
34. L. J. Yin, K. K. Bai, W. X. Wang, S. Y. Li, Y. Zhang, and L. He, Landau quantization of Dirac fermions in graphene and its multilayers, *Front. Phys.* 12(4), 127208 (2017)
35. S. Cho, Y. F. Chen, and M. S. Fuhrer, Gate-tunable graphene spin valve, *Appl. Phys. Lett.* 91(12), 123105 (2007)
36. Y. T. Zhang, Z. H. Qiao, and Q. F. Sun, Detecting zero-line mode in bilayer graphene via the quantum Hall effect, *Phys. Rev. B* 87(23), 235405 (2013)
37. M. Sui, G. Chen, L. Ma, W. Y. Shan, D. Tian, K. Watanabe, T. Taniguchi, X. Jin, W. Yao, D. Xiao, and Y. Zhang, Gate-tunable topological valley transport in bilayer graphene, *Nat. Phys.* 11(12), 1027 (2015)
38. L. Meng, Z. D. Chu, Y. Zhang, J. Y. Yang, R. F. Dou, J. C. Nie, and L. He, Enhanced intervalley scattering of twisted bilayer graphene by periodic AB stacked atoms, *Phys. Rev. B* 85(23), 235453 (2012)
39. V. Ryzhii, T. Otsuji, M. Ryzhii, V. Ya. Aleshkin, A. A. Dubinov, V. Mitin, and M. S. Shur, Vertical electron transport in van der Waals heterostructures with graphene layers, *J. Appl. Phys.* 117(15), 154504 (2015)
40. J. W. González, H. Santos, M. Pacheco, L. Chico, and L. Brey, Electronic transport through bilayer graphene flakes, *Phys. Rev. B* 81(19), 195406 (2010)
41. S. Das Sarma, S. Adam, E. H. Hwang, and E. Rossi, Electronic transport in two-dimensional graphene, *Rev. Mod. Phys.* 83(2), 407 (2011)
42. T. Nakanishi, M. Koshino, and T. Ando, Transmission through a boundary between monolayer and bilayer graphene, *Phys. Rev. B* 82(12), 125428 (2010)
43. L. Brey and H. A. Fertig, Electronic states of graphene nanoribbons studied with the Dirac equation, *Phys. Rev. B* 73(23), 235411 (2006)
44. I. Snyman and C. W. J. Beenakker, Ballistic transmission through a graphene bilayer, *Phys. Rev. B* 75(4), 045322 (2007)
45. H. M. Abdullah, B. Van Duppen, M. Zarenia, H. Bahlouli, and F. M. Peeters, Quantum transport across van der Waals domain walls in bilayer graphene, *J. Phys.: Condens. Matter* 29(42), 425303 (2017)
46. H. M. Abdullah, D. R. da Costa, H. Bahlouli, A. Chaves, F. M. Peeters, and B. Van Duppen, Electron collimation at van der Waals domain walls in bilayer graphene, *Phys. Rev. B* 100(4), 045137 (2019)
47. J. W. González, H. Santos, E. Prada, L. Brey, and L. Chico, Gate-controlled conductance through bilayer graphene ribbons, *Phys. Rev. B* 83(20), 205402 (2011)
48. H. Zheng, Z. F. Wang, T. Luo, Q. W. Shi, and J. Chen, Analytical study of electronic structure in armchair graphene nanoribbons, *Phys. Rev. B* 75(16), 165414 (2007)
49. H. Santos, A. Ayuela, W. Jaskólski, M. Pelc, and L. Chico, Interface states in carbon nanotube junctions: Rolling up graphene, *Phys. Rev. B* 80(3), 035436 (2009)
50. C. Berger, Z. Song, X. Li, X. Wu, N. Brown, C. Naud, D. Mayou, T. Li, J. Hass, A. N. Marchenkov, E. H. Conrad, P. N. First, and W. A. de Heer, Electronic confinement and coherence in patterned epitaxial graphene, *Science* 312(5777), 1191 (2006)
51. A. K. Geim and K. S. Novoselov, The rise of graphene, *Nat. Mater.* 6(3), 183 (2007)
52. X. Li, W. Cai, J. An, S. Kim, J. Nah, D. Yang, R. Piner, A. Velamakanni, I. Jung, E. Tutuc, S. K. Banerjee, L. Colombo, and R. S. Ruoff, Large-Area Synthesis of High-Quality and Uniform Graphene Films on Copper Foils, *Science* 324(5932), 1312 (2009)
53. K. S. Kim, Y. Zhao, H. Jang, S. Y. Lee, J. M. Kim, K. S. Kim, J. H. Ahn, P. Kim, J. Y. Choi, and B. H. Hong, Large-scale pattern growth of graphene films for stretchable transparent electrodes, *Nature* 457(7230), 706 (2009)
54. W. X. Wang, M. Zhou, X. Li, S. Y. Li, X. Wu, W. Duan, and L. He, Energy gaps of atomically precise armchair graphene sidewall nanoribbons, *Phys. Rev. B* 93, 241403(R) (2016)
55. J. Kunstmann, C. Özdogan, A. Quandt, and H. Fehske, Stability of edge states and edge magnetism in graphene nanoribbons, *Phys. Rev. B* 83(4), 045414 (2011)
56. L. Salemi, A. Lherbier, and J. C. Charlier, Spin-dependent properties in zigzag graphene nanoribbons with phenyl-edge defects, *Phys. Rev. B* 98(21), 214204 (2018)
57. S. Datta, Electronic Transport in Mesoscopic Systems, Cambridge University Press, Cambridge UK, 1997